

Quantum Chemistry Simulations of Dominant Products in Lithium-Sulfur Batteries

Julia E. Rice,¹ Tanvi P. Gujarati,¹ Tyler Y. Takeshita,² Joe Latone,¹
Mario Motta,¹ Andreas Hintennach,³ and Jeannette M. Garcia¹

¹IBM Almaden Research Center, 650 Harry Road, San Jose, CA 95120, USA

²Mercedes Benz Research and Development North America, Sunnyvale, CA 94085

³Daimler AG (Mercedes-Benz Cars), Group Research, HPC G012-BB, 71034, Boeblingen, Germany

Quantum chemistry simulations of four industrially relevant molecules are reported. Dissociation curves and dipole moments are reported for lithium hydride (LiH), hydrogen sulfide (H₂S), lithium hydrogen sulfide (LiSH) and lithium sulfide (Li₂S). Herein, we demonstrate the ability to calculate dipole moments using up to 21 qubits on a quantum simulator for a lithium sulfur salt molecule, and demonstrate the ability to calculate the dipole moment of the LiH molecule on the IBM Q Valencia device using four qubits. This is the first example to the best of our knowledge of dipole moment calculations being performed on quantum hardware.

INTRODUCTION

Lithium-sulfur batteries are a promising next-generation battery technology with a high theoretical capacity of up to ~ 1675 mAh/g and high theoretical energy density of ~ 2600 Wh/kg (Li-ion theoretical energy density is ~ 350 -500 Wh/kg) [1–3]. The reversible battery functioning is based on the electrochemistry between lithium metal (Li⁰) and elemental sulfur (S₈) to form lithium sulfide (Li₂S) as the thermodynamic product, as illustrated in Figure 1. The reduction of sulfur is known to proceed on discharge in the battery, through a series of intermediate lithium polysulfide salts, some of which are soluble in the electrolyte and can diffuse to the lithium metal anode. The solubility of various intermediates provides unique challenges for the realization of lithium-sulfur batteries and limits its potential use as a practical alternative to state-of-the-art lithium-ion chemistries.

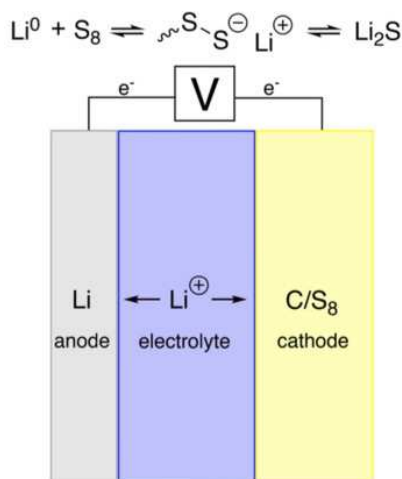


FIG. 1. The chemistry of a lithium-sulfur battery. During discharge, elemental sulfur is reduced into sulfur salts containing chains of varying lengths, ultimately resulting in lithium sulfide production. During charge, the chemistry is reversed. The mechanism for lithium sulfide production is proposed to occur through a two-electron process.

In order to harness control over the battery technology, the

mechanism for production and identification of reactive intermediates must be validated. However, the reaction mechanism for sulfur reduction in the battery environment is highly complex and debated in the field. Intermediates are difficult (if not impossible) to characterize during operation of the battery and competing chemical (vs electrochemical) pathways are also active, which confounds the mixture of products produced. Generally, products are assumed to be produced through either one electron or two electron processes, which generate radicals and Li-S salts, in which the sulfur anion consists of 1-8 sulfur atoms. Four electron processes have also been considered but are unlikely processes as there is little experimental evidence and for entropic reasons [4].

The electron-cloud density distribution of molecules, and particularly their dipole moment, are critical for understanding a variety of phenomena occurring in batteries. In general, molecules with high polarity can easily attract or repel valence electrons from other compounds and generate reactions through electron transfer. The dipole moment of a molecule also determines its response to an external electric field. Accurate computation of energetics and dipole moments of molecules is thus a problem with deep conceptual importance, and significant applicability to the chemistry of LiS batteries. Achieving this goal requires solving the Schrödinger equation for the molecules of interest, a problem that is known to be exponentially expensive for classical computers, unless approximation schemes are introduced.

Quantum computing is a mode of attack of mathematical problems, that has an enormous potential to provide advantage over conventional computing in a number of areas, including quantum chemistry [5–7]. A number of heuristics to provide approximate but highly accurate solutions to the Schrödinger equation have been proposed, in particular the Variational Quantum Eigensolver (VQE) [8–10]. IBM researchers have demonstrated the use and accuracy of VQE in investigations of a variety of molecules [11].

Motivated by these successes, and by the importance of computing energies and electrostatic properties, in this work we assess the performance of quantum algorithms in determining ground state energies and dipole moments along bond stretching for LiH, H₂S, LiSH and Li₂S.

The calculations presented here are important for the development of quantum computing: to the best of our knowledge, we present the first hard-ware simulation of dipole moments. Our results immediately generalize to expectation values of k -body operators in materials, with significant implications for the ability to study reactivity and electrostatics in batteries by quantum algorithms.

METHODOLOGY

The overall strategy for the calculations performed in this work involved initial preprocessing by classical quantum chemistry codes on conventional computers, to generate optimized mean-field orbitals and matrix elements of the Hamiltonian prior to performing computations with quantum simulators or devices. The restricted Hartree-Fock (RHF) singlet state has been chosen as the initial state for all of the calculations described here, since experience has indicated this state as a good choice for a variety of chemical problems [12]. Restricted coupled-cluster with singles and doubles (CCSD) calculations were performed using Psi4 [13], at STO-3G level of theory, using the frozen-core approximation for correlated calculations. The choice of the minimal basis is motivated by the fact that only a few molecular orbitals can be simulated on contemporary quantum hardware, since the number of available qubits is still relatively small, devices are noisy, and full quantum error correction techniques are not yet available. Additional details for the studied molecules are listed in Table I in the Supplemental Information.

Having selected a set of single-electron orbitals for each of the studied species, VQE computations were performed with quantum simulators and devices. We use IBM’s open-source Python library for quantum computing, Qiskit [14]. Qiskit provides tools for various tasks such as creating quantum circuits, performing simulations, and computations on real hardware. Qiskit Aqua contains an implementation of the VQE algorithm, a hybrid quantum-classical algorithm that uses both quantum and classical resources to solve the Schrödinger equation. It also provides a classical exact eigensolver algorithm (FCI) to compare results.

In the VQE algorithm, we take our wavefunction in the form of a quantum circuit, which is the unitary coupled cluster with singles and doubles (UCCSD) [15–17], its quantum variant (q-UCCSD) as defined in Ref [18] and the Ry variational form provided in Qiskit [14].

We then minimize the expectation value of the Hamiltonian with respect to the parameters of our circuit. The minimization is carried out through the classical optimization method, L_BFGS_B [19–21] on the simulator, and Simultaneous Perturbation Stochastic Approximation (SPSA) [22, 23] on the device. Once the VQE is complete, we get the optimized variational form and the upper bound for the ground state energy.

We ran our experiments on both the statevector and qasm simulators in Qiskit. We performed hardware experiments on IBMs Quantum Computation Centers new T-shaped 5-qubit

quantum processor, Valencia, where we employed readout-error mitigation using Qiskit Ignis to correct measurement errors. We also used a simple noise extrapolation scheme using additional CNOT gates at the minimum energy VQE iterations to account for errors introduced during the expensive 2-qubit entangling operations as was shown in Refs [24, 25].

RESULTS AND DISCUSSION

Quantum computing simulations on lithium-sulfur molecules

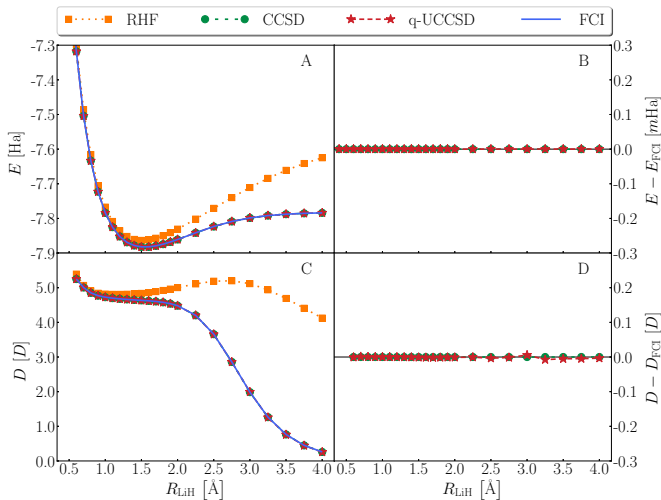


FIG. 2. Fig. 2 Calculations for lithium hydride, LiH. (A) Dissociation curve (ground state energy in Hartrees, as a function of interatomic distance, in angstroms) from RHF, CCSD, q-UCCSD and FCI. (B) Deviation from FCI energy, for CCSD and q-UCCSD, in millihartrees. (C) Dipole moment (in Debye) as a function of interatomic distance, in angstroms). (D) Deviation from FCI dipole moment, for CCSD and q-UCCSD, in Debye. Ha and D denote Hartree and Debye respectively.

The lithium hydride (LiH) bond can be represented by molecular (spatial) orbitals (MOs) with $2s$, $2p_z$ character for lithium and an MO with $1s$ character for hydrogen, for a total of 6 spin-orbitals. The ground state energy and dipole moments were calculated on the simulator through the use of six qubits and the hardware with four qubits after tapering [26, 27] techniques were applied.

As seen in Figure 2, results from CCSD, q-UCCSD and FCI coincide for both energy and dipole moment along bond stretching, due to the fact that CCSD and q-UCCSD are equivalent to FCI for two-electron systems. In the case of q-UCCSD some small deviations from FCI are observed. Of course, with molecules that contain more than two electrons, different results are observed for energies and other properties. Despite its simplicity, LiH has an interesting evolution in the dipole moment along the dissociation curve from a regime with ionic character (polar, short R) to one without polarity (large R).

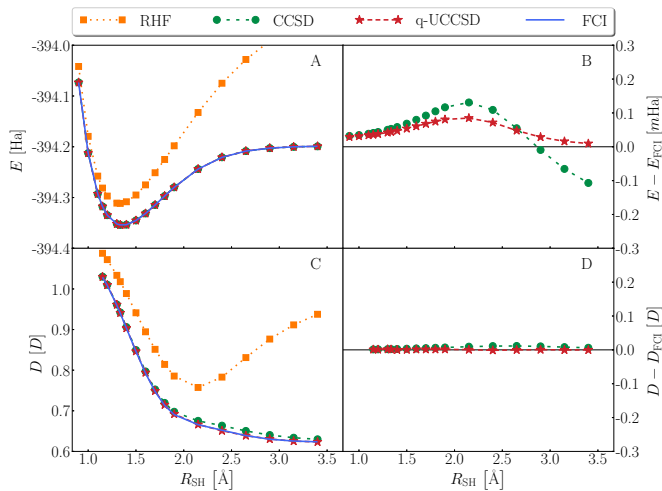


FIG. 3. Fig. 3 Calculations for hydrogen sulfide, H_2S . (A) Dissociation curve (ground state energy in Hartrees as a function of interatomic distance, in angstroms) from RHF, CCSD, q-UCCSD and FCI. (B) Deviation from FCI energy, for CCSD and q-UCCSD, in millihartrees. (C) Dipole moment (in Debye) as a function of interatomic distance, in angstroms). (D) Deviation from FCI dipole, for CCSD and q-UCCSD, in Debye. Ha and D denote Hartree and Debye respectively.

Hydrogen sulfide (H_2S) is represented by MOs with $3s$, $3p_x$, $3p_y$, $3p_z$, character for sulfur and an MO with $1s$ character for hydrogen, totaling 12 spin orbitals and 8 electrons. After employing tapering and qubit reductions to exploit symmetries in the molecule, the ground state energy and dipole moments were calculated on the simulator with 9 qubits. In Figure 3 we study the ground-state energy and dipole moment along bond stretching of H_2S , using CCSD, q-UCCSD and FCI. q-UCCSD and CCSD are in agreement with FCI across bond stretching (their maximum deviations from FCI being 0.13 and 0.8 millihartree respectively), with q-UCCSD providing a better estimate of the energy for large R_{HS} . The dipole moment is seen to monotonically decrease with R_{HS} towards ~ 0.6 D, and q-UCCSD values are in better agreement with FCI than CCSD ones (their maximum deviations from FCI being 1.7 millidebye and 11.5 millidebye respectively).

As seen in Figure 3, differences between q-UCCSD and FCI energies are always greater than zero. This can be understood, since the q-UCCSD energies are variational in nature [15–17] (only include singles and doubles) and are therefore above the FCI values. It is also understandable that the most challenging regime is the intermediate dissociation regime, where the ground-state wavefunction switches between different dominant determinants in its configuration interaction expansion, exhibiting multireference character. Lithium sulfide (Li_2S) is represented by MOs with $3s$, $3p_x$, $3p_y$, $3p_z$, character for sulfur and $2s$, $2p_x$, $2p_y$, $2p_z$, character for lithium, for a total of 24 spin orbitals and 8 electrons. After employing tapering and qubit reductions to account for molecular symmetries, the ground state energy and dipole moments were calculated on the simulator with 21 qubits. UCCSD and CCSD

estimates for energy and dipole are similar in accuracy along bond stretching.

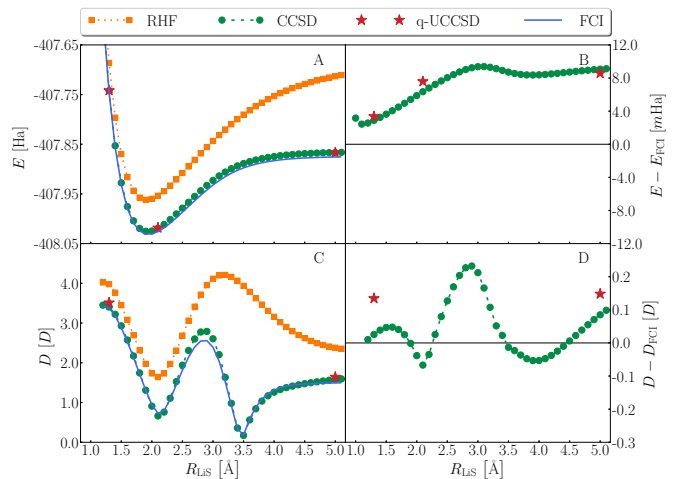


FIG. 4. Calculations for lithium sulfide, Li_2S . (A) Dissociation curve (ground state energy in Hartrees as a function of interatomic distance, in angstroms) from RHF, CCSD, q-UCCSD and FCI. (B) Deviation from FCI energy, for CCSD and q-UCCSD, in millihartrees. (C) Dipole moment (in Debye) as a function of interatomic distance, in angstroms). (D) Deviation from FCI dipole, for CCSD and q-UCCSD, in Debye. Ha and D denote Hartree and Debye respectively.

Lithium hydrogen sulfide (LiSH) is represented by MOs with $3s$, $3p_x$, $3p_y$, $3p_z$, character for sulfur, $1s$ character for hydrogen and $1s$, $2s$, $2p_x$, $2p_y$, $2p_z$, character for lithium, for a total of 18 spin orbitals and 8 electrons. After employing tapering and qubit reductions possible due to symmetry [26, 27], the ground state energy and dipole moments were calculated on the simulator with 15 qubits.

Results are shown in Figures 5 and 6. In Figure 5, the dissociation of the LiS bond is studied by varying R_{LiS} with all other internal coordinates fixed at their experimental [28] values. For all but the largest values of R_{LiS} , CCSD is in better agreement with FCI for both the energy and the dipole moment. As in the H_2S case, the most challenging regime is the intermediate dissociation region, where the energy is overestimated by 5 millihartrees and the dipole moment by $\sim 20\%$.

A very different situation is seen for the dissociation of the covalent SH bond, illustrated in Figure 6. Description of the dissociation regime is more challenging for both CC flavors than that seen for the breaking of the Li-S bond, with q-UCCSD again performing better at large bond length. The FCI dipole moment decreases monotonically with R_{SH} , a tendency that both CC flavors correctly reproduce at a qualitatively, but not quantitatively for large bond length. In both cases, deviations from FCI signal the limited accuracy of the underlying ansatz, and take place in the intermediate dissociation regime.

Comparison between hydrogen-sulfur and lithium-sulfur bond stretching in LiSH reveals interestingly different behaviors. In particular, when the dipole moment is plotted

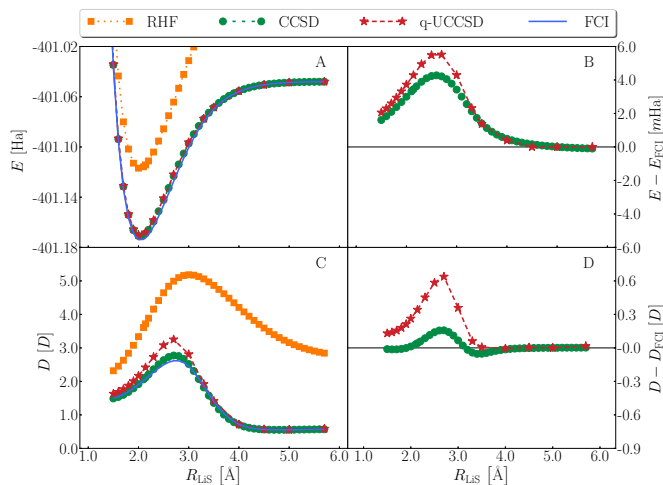


FIG. 5. Simulations of lithium hydrogen sulfide, LiSH, when breaking the Li-S bond. (A) Dissociation curve (ground state energy in Hartrees as a function of interatomic distance, in angstroms) from RHF, CCSD, q-UCCSD and FCI. (B) Deviation from FCI energy, for CCSD and q-UCCSD, in millihartrees. (C) Dipole moment (in Debye) as a function of interatomic distance, in angstroms). (D) Deviation from FCI dipole, CCSD and q-UCCSD, in Debye. Ha and D denote Hartree and Debye respectively.

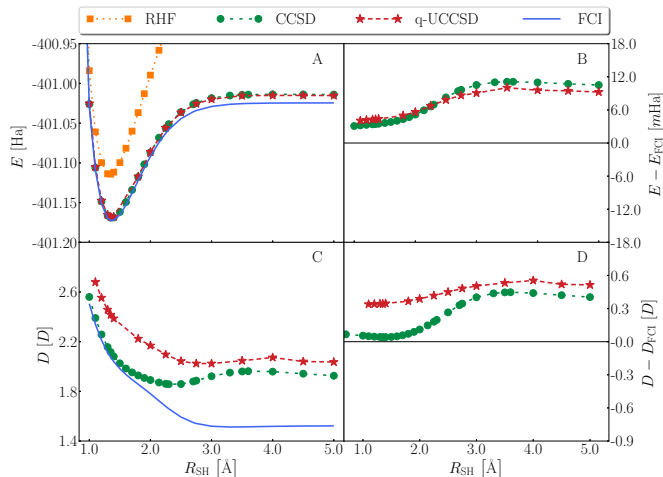


FIG. 6. Simulations of lithium hydrogen sulfide, LiSH, when breaking the S-H bond. (A) Dissociation curve (ground state energy in Hartrees as a function of interatomic distance, in angstroms) from RHF, CCSD, q-UCCSD and FCI. (B) Deviation from FCI energy, for CCSD and q-UCCSD, in millihartrees. (C) Dipole moment (in Debye) as a function of interatomic distance, in angstroms). (D) Deviation from FCI dipole, CCSD and q-UCCSD, in Debye. Ha and D denote Hartree and Debye respectively.

against the interatomic distance, very different behaviors are observed. For instance, no maximum value is observed between ~ 2.5 - 3.0 Angstroms for S-H bond stretching; instead, a change in slope closer to ~ 2.0 Angstroms is visible. We reason that the differences observed result from a difference in the nature of the bond as Li-S is ionic in character whereas S-H is covalent.

Quantum chemistry simulations on quantum devices

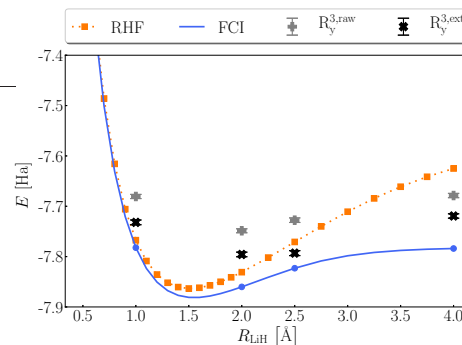


FIG. 7. Hardware-simulated ground-state energy calculations for LiH on the IBM Q Valencia device (energy in Hartrees as a function of interatomic distance, in angstroms). Ha denotes Hartree.

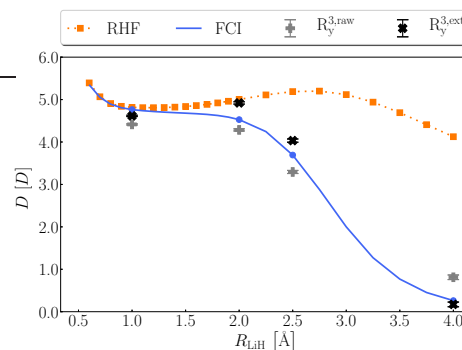


FIG. 8. Hardware-simulated dipole moment calculations for LiH on the IBM Q Valencia device (dipole moment in Debye, as a function of interatomic distance, in angstroms). D denotes Debye.

Next, the dipole moment of lithium hydride was evaluated using quantum hardware as described in the Methods section. We employ the hardware-efficient Ry ansatz to estimate the ground-state energy and dipole moment at three representative values of R . We employed a depth=3 circuit with CX entangling gates with linear connectivity. To the best of our knowledge, these are the first evaluations of dipole moments by quantum hardware simulations.

We chose to study four bond lengths representative of the polar and dissociation regimes. Results from hardware simulations in presence of noise are shown. A Richardson extrapolation [29, 30] is also conducted, with the aim of mitigating the impact of noise. As seen in Figures 7 and 8, the qualitative behavior of both energies and dipoles is correctly captured by the hardware simulations upon extrapolation. In particular, the dipole moment is accurate within $\sim 10\%$ in the polar regime. Future research will explore approaches to improve these results quantitatively, for example by the use of circuits with higher depth, by the exploration of multiple ansatzes or by the use of different error mitigation techniques.

CONCLUSIONS

Herein, we have reported on the simulations of four molecules (LiH, H₂S, LiSH and Li₂S) that increase in complexity to Li₂S which is relevant to the study of lithium-sulfur batteries. We showed that we could obtain ground state energies for each of these molecules within chemical accuracy on a quantum simulator using 6, 9, 15, and 21 qubits respectively. Preliminary results on lithium sulfide (Li₂S) are included.

Differences could be observed in the LiSH molecule depending on whether the hydrogen or lithium atom was dissociated from the sulfur atom. We hypothesize that these differences can be explained due to the difference in ionic compared to covalent character of the bond. Furthermore, the effects of electronic distribution changes could be observed when evaluating the dipole moment of lithium hydride. Additionally, we showed that the lithium hydride dipole moment could be qualitatively simulated on quantum hardware with four qubits.

This is a notable demonstration of the capabilities of the hardware since the dipole moment of lithium hydride changes from strongly polarized in its ionic state to effectively neutral at long bond distances over ~ 2.5 Å, representing a highly entangled state at this distance.

In the future, these methods can be applied to larger calculations on polyanions formed upon discharge in the Li-S battery to help evaluate between radical and ionic mechanisms of the electrochemical reduction of sulfur to lithium sulfide with lithium metal.

ACKNOWLEDGMENTS

The authors gratefully acknowledge helpful discussions with Eunseok Lee (MBRDNA), as well as Donny Greenberg, Marco Pistoia, and Stephen Wood (IBM).

-
- [1] R. Van Noorden, *Nature* **498**, 416 (2013).
- [2] D. Zheng, X. Zhang, J. Wang, D. Qu, X. Yang, and D. Qu, *Journal of Power Sources* **301**, 312 (2016).
- [3] P. Gibot, M. Casas-Cabanas, L. Laffont, S. Levasseur, P. Carlach, S. Hamelet, J.-M. Tarascon, and C. Masquelier, *Nature Materials* **7**, 741 (2008).
- [4] K. H. Wujcik, D. R. Wang, A. A. Teran, E. Nasybulin, T. A. Pascal, D. Prendergast, and N. P. Balsara, "Determination of redox reaction mechanisms in lithium-sulfur batteries," in *Electrochemical Engineering* (John Wiley & Sons, Ltd, 2018) Chap. 3, pp. 41–74.
- [5] I. M. Georgescu, S. Ashhab, and F. Nori, *Rev. Mod. Phys.* **86**, 153 (2014).
- [6] I. Kassal, J. D. Whitfield, A. Perdomo-Ortiz, M.-H. Yung, and A. Aspuru-Guzik, *Annual Review of Physical Chemistry* **62**, 185 (2011), PMID: 21166541.
- [7] Y. Cao, J. Romero, J. P. Olson, M. Degroote, P. D. Johnson, M. Kieferová, I. D. Kivlichan, T. Menke, B. Peropadre, N. P. D. Sawaya, S. Sim, L. Veis, and A. Aspuru-Guzik, *Chemical Reviews* **119**, 10856 (2019).
- [8] A. Peruzzo, J. McClean, P. Shadbolt, M.-H. Yung, X.-Q. Zhou, P. J. Love, A. Aspuru-Guzik, and J. L. O'Brien, *Nature Communications* **5**, 4213 (2014).
- [9] A. Kandala, A. Mezzacapo, K. Temme, M. Takita, M. Brink, J. M. Chow, and J. M. Gambetta, *Nature* **549**, 242 (2017).
- [10] P. J. Ollitrault, A. Kandala, C.-F. Chen, P. K. Barkoutsos, A. Mezzacapo, M. Pistoia, S. Sheldon, S. Woerner, J. Gambetta, and I. Tavernelli, [arXiv:1910.12890](https://arxiv.org/abs/1910.12890) (2019).
- [11] Q. Gao, H. Nakamura, T. P. Gujarati, G. O. Jones, J. E. Rice, S. P. Wood, M. Pistoia, J. M. Garcia, and N. Yamamoto, [arXiv:1906.10675](https://arxiv.org/abs/1906.10675) (2019).
- [12] J. Romero, R. Babbush, J. R. McClean, C. Hempel, P. J. Love, and A. Aspuru-Guzik, *Quantum Science and Technology* **4**, 014008 (2018).
- [13] J. M. Turney, A. C. Simmonett, R. M. Parrish, E. G. Hohenstein, F. A. Evangelista, J. T. Fermann, B. J. Mintz, L. A. Burns, J. J. Wilke, M. L. Abrams, N. J. Russ, M. L. Leininger, C. L. Janssen, E. T. Seidl, W. D. Allen, H. F. Schaefer, R. A. King, E. F. Valeev, C. D. Sherrill, and T. D. Crawford, *WIREs Computational Molecular Science* **2**, 556 (2012).
- [14] G. Aleksandrowicz, T. Alexander, P. Barkoutsos, L. Bello, Y. Ben-Haim, D. Bucher, F. Cabrera-Hernández, J. Carballo-Franquis, A. Chen, C. Chen, *et al.*, *Zenodo* **16** (2019).
- [15] W. Kutzelnigg, *The Journal of Chemical Physics* **77**, 3081 (1982).
- [16] W. Kutzelnigg and S. Koch, *The Journal of Chemical Physics* **79**, 4315 (1983).
- [17] W. Kutzelnigg, *The Journal of Chemical Physics* **82**, 4166 (1985).
- [18] P. K. Barkoutsos, J. F. Gonthier, I. Sokolov, N. Moll, G. Salis, A. Fuhrer, M. Ganzhorn, D. J. Egger, M. Troyer, A. Mezzacapo, S. Filipp, and I. Tavernelli, *Phys. Rev. A* **98**, 022322 (2018).
- [19] R. H. Byrd, P. Lu, J. Nocedal, and C. Zhu, *SIAM Journal on Scientific Computing* **16**, 1190 (1995).
- [20] C. Zhu, R. H. Byrd, P. Lu, and J. Nocedal, *ACM Trans. Math. Softw.* **23**, 550560 (1997).
- [21] J. L. Morales and J. Nocedal, *ACM Trans. Math. Softw.* **38**, 7 (2011).
- [22] J. C. Spall, *Johns Hopkins apl technical digest* **19**, 482 (1998).
- [23] J. C. Spall, in *Proceedings of the 37th IEEE Conference on Decision and Control*, Vol. 4 (1998) pp. 3872–3879 vol.4.
- [24] E. F. Dumitrescu, A. J. McCaskey, G. Hagen, G. R. Jansen, T. D. Morris, T. Papenbrock, R. C. Pooser, D. J. Dean, and P. Lougovski, *Phys. Rev. Lett.* **120**, 210501 (2018).
- [25] N. Stamatopoulos, D. J. Egger, Y. Sun, C. Zoufal, R. Iten, N. Shen, and S. Woerner, [arXiv:1905.02666](https://arxiv.org/abs/1905.02666) (2019).
- [26] S. Bravyi, J. M. Gambetta, A. Mezzacapo, and K. Temme, [arXiv preprint arXiv:1701.08213](https://arxiv.org/abs/1701.08213) (2017).
- [27] K. Setia, R. Chen, J. E. Rice, A. Mezzacapo, M. Pistoia, and J. Whitfield, [arXiv preprint arXiv:1910.14644](https://arxiv.org/abs/1910.14644) (2019).
- [28] R. D. Johnson III, *NIST 101. Computational chemistry comparison and benchmark database*, Tech. Rep. (1999).
- [29] K. Temme, S. Bravyi, and J. M. Gambetta, *Phys. Rev. Lett.* **119**, 180509 (2017).
- [30] A. Kandala, K. Temme, A. D. Córcoles, A. Mezzacapo, J. M. Chow, and J. M. Gambetta, *Nature* **567**, 491 (2019).

APPENDIX

species	geometry	equilibrium values	symmetry	spin-orbitals	qubits	frozen orbitals
LiH	Li(0, 0, 0) H(0, 0, R_{LiH})	$R_{\text{LiH}} = 1.595 \text{ \AA}$	$C_{\infty v}$	6	4	Li(1s, 2p _x , 2p _y)
H ₂ S	S(0, 0, 0) H($R_{\text{SH}} \cos(\theta_{\text{HSH}}), R_{\text{SH}} \sin(\theta_{\text{HSH}}), 0$) H($-R_{\text{SH}} \cos(\theta_{\text{HSH}}), R_{\text{SH}} \sin(\theta_{\text{HSH}}), 0$)	$R_{\text{SH}} = 1.356 \text{ \AA}$ $\theta_{\text{HSH}} = 92.11^\circ$	C_{2v}	12	9	S(1s, 2s, 2p)
Li ₂ S	S(0, 0, 0) Li($R_{\text{LiS}} \cos(\theta_{\text{LiSLi}}), R_{\text{LiS}} \sin(\theta_{\text{LiSLi}}), 0$) Li($-R_{\text{LiS}} \cos(\theta_{\text{LiSLi}}), R_{\text{LiS}} \sin(\theta_{\text{LiSLi}}), 0$)	$R_{\text{LiS}} = 2.140 \text{ \AA}$ $\theta_{\text{LiSLi}} = 134.97^\circ$	C_{2v}	24	21	S(1s, 2s, 2p)
LiSH	S(0, 0, 0) Li($R_{\text{LiS}}, 0, 0$) H($R_{\text{SH}} \cos(\theta_{\text{LiSH}}), R_{\text{SH}} \sin(\theta_{\text{LiSH}}), 0$)	$R_{\text{LiS}} = 2.140 \text{ \AA}$ $R_{\text{SH}} = 1.353 \text{ \AA}$ $\theta_{\text{LiSH}} = 92.11^\circ$	C_s	18	15	Li(1s) S(1s, 2s, 2p)

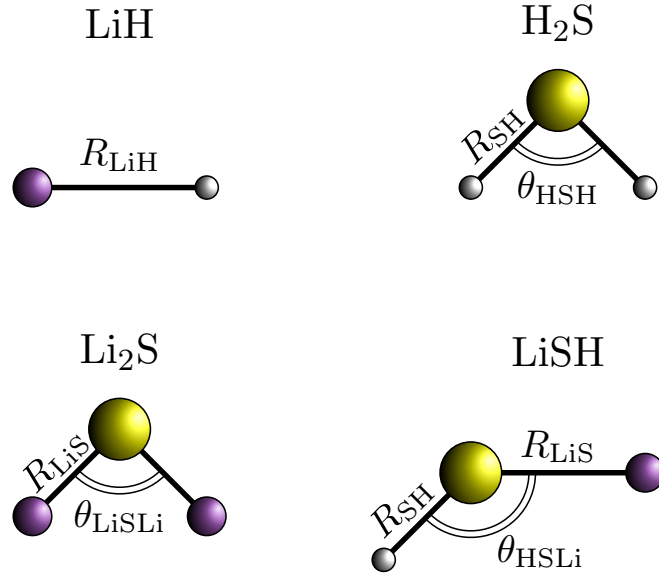


TABLE I. Table: List of the chemical species investigated in the present work. For each species, we list the investigated geometries, specified in terms of internal coordinates. Whenever internal coordinates are fixed at chosen values, the latter correspond with the quantities listed in column 3. For each species we show the frozen orbitals, molecular symmetry group and number of spin-orbitals and qubits. Figure: pictorial representation of the chemical species and geometries studied in the present work; white, purple and yellow spheres represent H, Li and S atoms respectively.